Three-dimensional numerical modeling of photonic integration with dielectric-loaded SPP waveguides

A. V. Krasavin* and A. V. Zayats
Centre for Nanostructured Media, IRCEP, The Queen's University of Belfast, Belfast BT7 1NN, United Kingdom
(Received 4 April 2008; revised manuscript received 30 April 2008; published 22 July 2008)

Using full three-dimensional numerical modeling, we demonstrate highly efficient passive and active photonic circuit elements based on dielectric-loaded surface plasmon polariton waveguides (DLSPPWs). Highly confined surface plasmon polariton (SPP) mode having subwavelength cross section allows high level of integration of DLSPPW circuitry. We demonstrate very efficient guiding and routing of SPP signals with the passive waveguide elements such as bends, splitters, and Bragg reflectors, having a functional size of just a few microns at telecommunication wavelengths. Introducing a gain in the dielectric, we have found the requirement for lossless waveguiding and estimated the performance of DLSPPW lossless and active elements. DLSPPW based components have prospective implementation in photonic integrated chips, hybrid optical-electronic circuits, and lab-on-a-chip applications.

DOI: 10.1103/PhysRevB.78.045425 PACS number(s): 73.20.Mf, 71.36.+c, 42.82.−m, 42.79.Ta

I. INTRODUCTION

Surface plasmon polaritons (SPPs) have proved to be very efficient for confinement and guiding of optical signals on subwavelength scale. They are widely considered as a prospective type of optical information carrier in highly integrated photonic devices. Moreover, due to the SPP field confinement and enhancement near the metal interface, various functionalities can be efficiently implemented with SPPs through nonlinear electro-optical or thermo-optical effects.

A surface plasmon polariton is an electromagnetic wave coherently coupled to electron oscillations and propagating in a wavelike fashion along a metal-dielectric interface.[1] Being a surface wave, a SPP is intrinsically confined near the metal surface, exponentially decaying from it at a subwavelength distance in dielectric and in metal. A variety of two-dimensional optical elements for surface polaritons, such as mirrors, lenses, resonators, sources, detectors, etc., has been demonstrated.[2] Moreover, it is possible to implement various SPP waveguiding structures, such as metallic stripes and wires,[3–5] grooves (gaps) in a metal surface,[6,7] metallic wedges,[8] a chain of metallic nanoparticles,[9] and metal heterostructures.[10] A SPP wave, however, experiences attenuation as it propagates due to Ohmic losses in the metal. Several approaches to increase SPP propagation length have been developed using long-range SPP modes[5] or SPP amplification.[11] The concept of active plasmonics for switching and modulating of SPP waves all optically or electronically has been also proposed.[5,12–15] These developments facilitate various possible applications of SPPs in telecommunication networks, integrated photonics, and lab-on-a-chip systems.

Of all the guiding approaches, metallic stripe waveguides have been primarily investigated. They provide relatively large SPP propagation distance up to the centimeter range. However, they require quite a large (>1 mm) radius of waveguide bending elements to have reasonable bend losses.[16,17] In order to achieve smaller bend losses, dielectric ridge SPP waveguides on a metal surface [dielectric-loaded SPP waveguides (DLSPPWs)] have been implemented recently[18–23] [Fig. 1(a)]. The refractive index for SPP wave on the metal-dielectric interface is significantly higher than on the outer air-metal interface, which leads to the formation of SPP mode analogous to the optical mode in the conventional optical fiber or planar dielectric waveguides. High refractive index contrast between the mode and the free-propagating SPP wave on the outer metal surface as well as light in the surrounding space leads to strong guiding properties of DLSPPW. This allows bending and splitting waveguide elements to be just a few micrometers long at telecommunication wavelengths.[21] The advantage of DLSPPW compared to other SPP waveguide types is that a dielectric ridge can be easily functionalized to provide thermo-optical, electro-optical, or all-optical functionalities and can be used for the development of active plasmonic components. Several approaches, such as direct laser writing on a spin-coated polymer followed by wet etching[18] and standard photolithography or electron-beam lithography[22,23] have been proven to be efficient in fabrication of high-quality DLSPPW structures [Fig. 1(a)]. In the recent developments, the nanoimprint technique is also showing good results and is under extensive development.[24]

Here, using full three-dimensional (3D) finite-element numerical simulations, we extended our investigation of guiding properties of dielectric-loaded SPP waveguides started in Ref. 21 as well as estimated the performance of DLSPPW active elements. We discussed an achievable level of photonic integration density based on DLSPPW circuitry and demonstrated efficient manipulation of SPP signals in a wide range of passive DLSPPW components. By introducing a gain in the dielectric, we found the requirement for the lossless propagation of the guided mode and studied the performance of lossless waveguide elements. Finally, we analyzed the performance of active waveguide elements, such as Mach-Zehnder interferometer (MZI) and a gain element, which can play a role of amplifying component and switch and/or modulator.

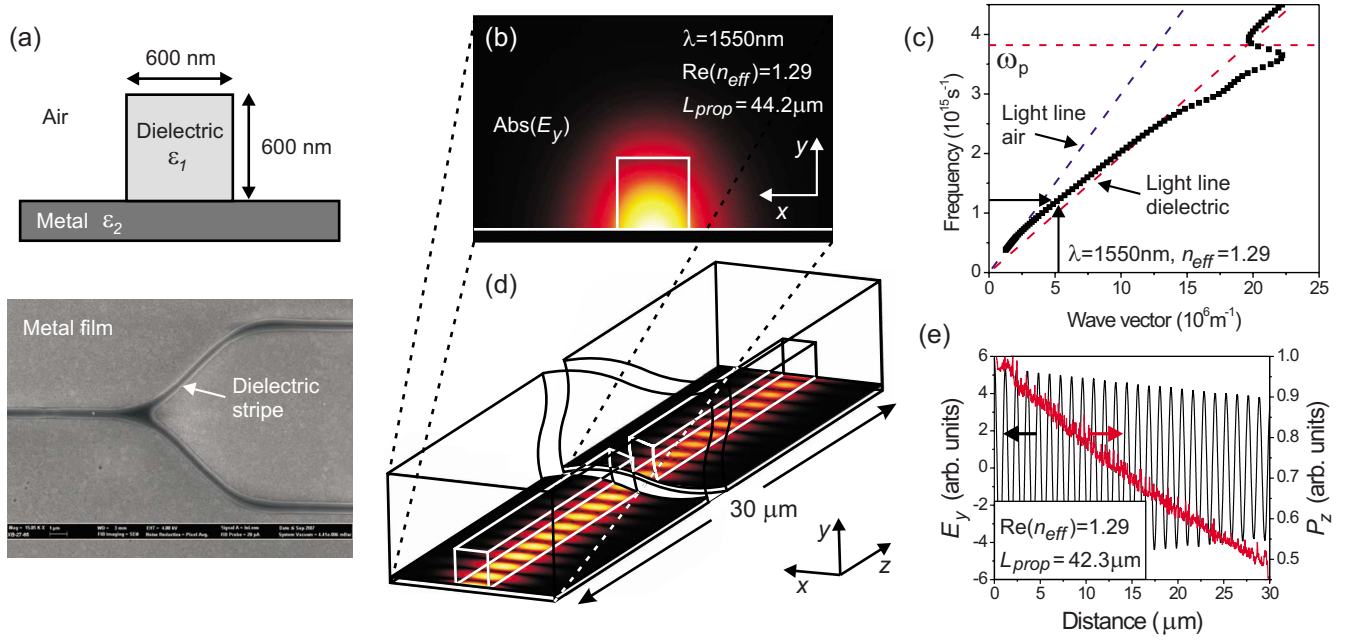

FIG. 1. (Color online) (a) Top: cross section of DLSPP waveguide and bottom: scanning electron microscopy image of the DLSPP waveguide fabricated by the technique of deep ultraviolet lithography described in Ref. 22. (b) abs(E_y) field profile of a fundamental TM_{00} SPP mode in 600×600 nm^2 DLSPP waveguide at $\lambda=1550$ nm. (c) Dispersion of TM_{00} SPP mode in the waveguide. (d) Simulation setup and abs(E_y) field distribution in a straight DLSPP waveguide. (e) Vertical component of the electric field E_y and power flow component P_z along the center of the waveguide at a distance of 10 nm from the metal surface.

II. MODE ANALYSIS AND ACHIEVABLE PHOTONIC INTEGRATION

We modeled a dielectric (e.g., polymer with $\epsilon_1=2.36$) stripe DLSPP waveguide with cross section of 600×600 nm^2 deposited onto a gold surface (ϵ_2, taken from Ref. 25, e.g., $\epsilon_2=-132+12.65i$ at $\lambda=1550$ nm) [see Fig. 1(a)]. Practically, the metal component can be a film deposited on a substrate; however, we found that for a gold film thickness larger than 100 nm the SPP mode does not feel the presence of the substrate. So the modeling of the substrate can be omitted to reduce the numerical complexity of the model by reducing the number of mesh elements.

First we performed two-dimensional (2D) eigenmode simulations, studying mode characteristics of the waveguide. At wavelengths above ~1250 nm, a waveguide of these dimensions is single mode for SPP waves supporting the fundamental TM_{00} mode, which is consistent with calculations made in Ref. 20. The mode is highly localized in the dielectric core of the waveguide at the metal-dielectric interface [Fig. 1(b)]. Studying the mode parameters at various wavelengths, we found the dispersion characteristic of the mode and the mode profiles corresponding to different frequencies [Fig. 1(c)]. At lower frequencies, more energy of the mode is located in the air region; therefore, the mode dispersion is close to the SPP dispersion at the metal-air interface. At higher frequencies, more energy is inside the dielectric; consequently, the mode dispersion follows the SPP dispersion at the metal-dielectric interface crossing the light line at the surface plasmon frequency ω_p of the metal-dielectric interface. For the following simulations we use a telecommunication wavelength $\lambda=1550$ nm, where only one SPP mode, TM_{00}, is supported. Moreover at this wavelength, the chosen geometrical parameters of the waveguide provide the optimum ratio between mode confinement and propagation.[20] The propagation characteristics were estimated from a complex value of the mode effective refractive index, which gives $\mathrm{Re}(n_{\mathrm{eff}})=1.29$ and $L_{\mathrm{prop}}^{2D}=44.2$ μm (the length at which energy of SPP decays in e times due to Ohmic losses). This propagation length corresponds to a propagation loss of 18 dB/cm.

We proceed with full 3D DLSPPW simulations, setting the SPP field distribution found in the 2D eigenmode simulations as a source boundary condition [Figs. 1(b) and 1(d)]. We started from a simple case of a straight waveguide, which gives us an opportunity to compare the mode propagation with the above results. On this example the validity of 3D simulation has been proved: the mode propagated along the waveguide in the single mode regime with essentially the same propagation characteristics as were found in 2D eigenmode simulations [Fig. 1(e)]. Here the precision of 3D simulations have been improved in comparison with Ref. 21. After this we are ready to simulate waveguide elements requiring simulation in 3D.

The key question in proposing a new type of photonic circuit is the level of integration achievable using implemented guiding approach. We investigated a cross-talk between two parallel DLSPP waveguides placed at a small distance from each other [Fig. 2(a)]. The critical separation parameter can be found from the condition $L_c\sim L_{\mathrm{prop}}$, which for telecommunication wavelength range corresponds to about 1.5 μm distance between the centers of the waveguides. We define the achievable level of integration as $L_c\gg L_{\mathrm{prop}}$. We found that at a distance $d=2.6$ μm, the cou-

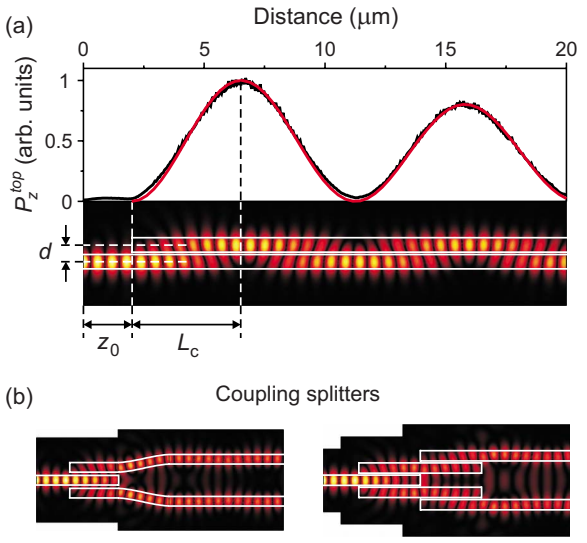

FIG. 2. (Color online) (a) DLSPPW mode oscillation between two coupled waveguides separated by a distance $d=700$ nm. The graph shows the power flow P_z along the axis of the top waveguide, 10 nm from the metal surface. The black line corresponds to the simulation results and red (gray) curve corresponds to the fitting of the data with a formula $P_z^{top}=P_{z0}\{1-\cos[2\pi/L_c(z-z_0)]\}\exp(-z/L_{prop})$. (b) Simulated splitters based on coupled DLSPP waveguides.

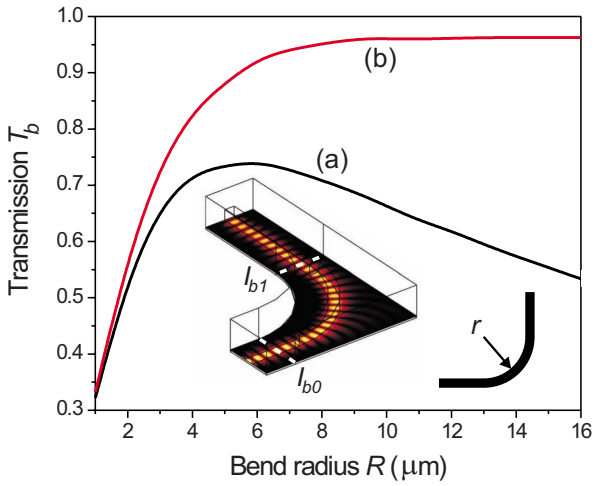

FIG. 3. (Color online) Performance of a 90° circular waveguide bend as a function of its radius r. Curve (a) corresponds to dielectric with $\epsilon_1=2.36$ and curve (b) corresponds to optical gain dielectric with $\epsilon_1=2.36+0.00944i$. The inset shows the simulation setup.

pling length L_c is 2.3 mm, so the waveguides are practically not coupled. In this case, after propagation of 200 μm, when the intensity of the mode decreases more than 100 times, less than 0.5% of the mode energy tunneled into the neighboring waveguide. This leads to a high level of integration of the photonic circuit on the basis of DLSPPW. At extremely small distances between the waveguides, the coupling is strong, for example, at $d=700$ nm [the case shown in Fig. 2(a)], the coupling distance is $L_c=4.63$ μm. This can be used in designs of such elements as waveguide splitters [see Fig. 2(b), this will be discussed in detail in Sec. III B]. For more information about waveguide-to-waveguide coupling, see Ref. 21.

III. PASSIVE WAVEGUIDE ELEMENTS

A. Waveguide bends

We continue with the modeling of the first elemental structure required to build DLSPP waveguide circuitry, a 90° waveguide bend. We implemented it by curving the waveguide along a circular arc of a radius r of several micrometers (see the inserts in Fig. 3). The modeled near-field distributions show that as the mode propagates along the curved section, it experiences radiation losses in the form of the SPPs on the surface outside the waveguide and a free space light.[21] We define the transmission through the bend T as a ratio between the power flow integrals in the dielectric core of the waveguide at the beginning I_{b0} and at the end I_{b1} of the bend section, $T_b=I_{b1}/I_{b0}$. The actual integrals calculated in this and further models were set in the very front and the very end edges of the waveguide, then the power flow in the beginning and the end of the bending or splitting sections was calculated using a known propagation length. Also the integrals were calculated not over the whole domain edge but only over the dielectric ridge region, the total power flow value being reconstructed using the coefficients found in the 2D eigenmode simulations. These two approaches are introduced to exclude the influence of scattered waves on the waveguide transmission integrals. The integrals were calculated using a standard expression for power flow, e.g., $I_z=0.5\int \mathrm{Re}(E_xH_y^*-E_yH_x^*)dxdy$. The dependence of transmission T on the radius of the bend r [Fig. 3, curve (a)] is defined by a trade-off between two sources of losses. For small bend radii (sharp bends), radiation losses play the dominating role. This can be understood from the observation that on the outer edge of the bend the DLSPPW mode becomes coupled to both the free propagating SPP wave on the metal surface and/or a light wave. For large radii, where the radiation losses are small, the absorption Ohmic losses become dominant due to the increase in the length of the bend section. At the optimal value of bend radius $R\sim 5$ μm, when the total losses of the bend are minimal, the transmission is as much as 75% (or a signal loss of 1.3 dB). Moreover if the losses in metal are compensated, the transmission can be above 95%; this case will be studied below in detail. Importantly, the size of the bend element based on DLSPPW is much smaller than in the case of planar dielectric waveguide and metallic stripe waveguide approaches.[16,17,26]

Another type of bending element for DLSPPW circuitry is an S-shaped waveguide bend (see insets in Fig. 4). The step value D was chosen to be 2.6 μm in line with the integration density found above. We studied three different shapes of the curved sections of the bend. Following Ref. 26 where the optimal shapes for S bends of the planar dielectric optical waveguides were discussed, we used the shape of curved sections given by [case (i)] $D/2(1-\cos(\pi z/L_s))$ and [case (ii)] $D/L_s\cdot z-D/(2\pi)\cdot\sin(2\pi z/L_s)$. Case (iii) corresponds to the S bend constructed of two circular arcs, whose radius and angle span were adjusted to provide the desirable step and length of the bend as well as smooth connection at the junction point. The performance of the S bend was studied as a

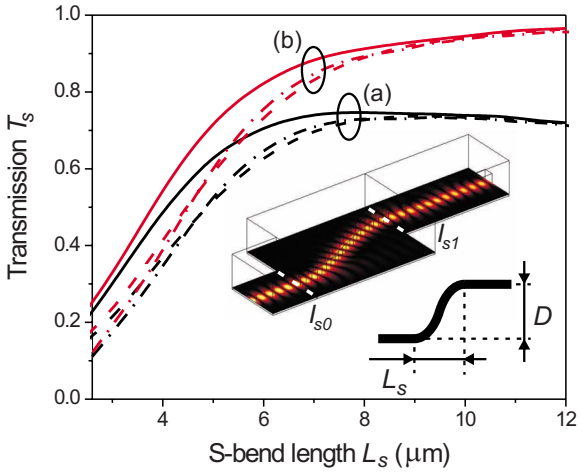

FIG. 4. (Color online) Dependence of the transmission T_s through a S-shaped waveguide bend with a step $D=2.6$ μm on the S-bend length L_s for three shapes described in text: (i) solid line, (ii) dashed line, and (iii) dash-dotted line. Group (a) correspond to dielectric with $\epsilon_1=2.36$ and group (b) correspond to dielectric with gain, having $\epsilon_1=2.36+0.00944i$. The inset shows the simulation setup.

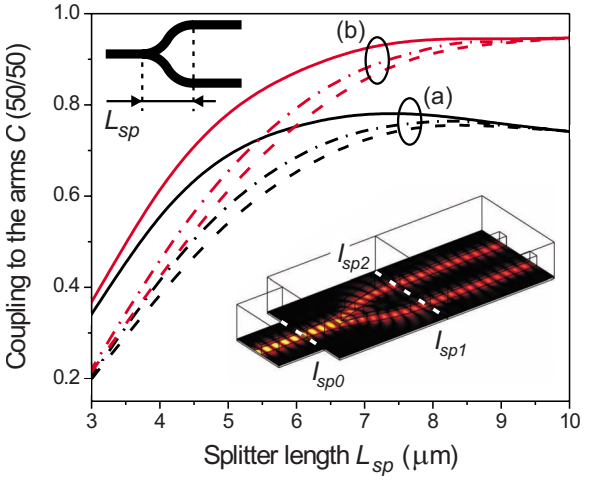

FIG. 5. (Color online) Efficiency C of the fork-shaped splitter with the output arm separation of 2.6 μm as a function of the length of the splitting element L_{sp} for three shapes described in text: (i) solid line, (ii) dashed line, and (iii) dash-dotted line. Group (a) correspond to dielectric with $\epsilon_1=2.36$ and group (b) correspond to gain dielectric with $\epsilon_1=2.36+0.00944i$. The inset shows the simulation setup.

function the S-bend element length L_s (see Fig. 4). The pure harmonic shape of the curved sections [case (i)] gives slightly larger values of the transmission in comparison with the other two, generally showing similar results. The optimal S-bend element with a length of 8 μm provides the transmission as big as $T=0.75$.

B. Splitters

A key element in the integrated optical circuits is a waveguide splitter. We simulated the DLSPPW splitter having several geometries, starting from the most straightforward fork-shaped splitter (see the inset in Fig. 5). The separation between the output arms was set to 2.6 μm to ensure their optical isolation from each other. The efficiency of the splitter C was optimized by varying the length of the splitting region L_{sp} (Fig. 5) for three shapes of the splitter arms. The shapes were defined by the same profiles as in the S-bend simulations. The efficiency was calculated as $C=(I_{sp1}+I_{sp2})/I_{sp0}$, where I_{sp0}, I_{sp1}, and I_{sp2} are power flow integrals in the dielectric cores at the beginning and at the end of the splitter output arms. Due to the symmetry of the splitter, the input mode energy is divided into two equal parts, $I_{sp1}=I_{sp2}$. The performance of the splitter is defined by the same trade-off between radiation and Ohmic losses as in the case of 90° waveguide bend or S bend. However, for the similar performance in the case of the splitter, the transverse step of each arm is $2.6/2$ μm$=1.3$ μm, compared to 2.6 μm in the S-bend case. Thus, the arms of the splitter should be two times "smoother." This is explained by the fact that in the case of a splitter, there are additional radiation losses increasing with the splitter becoming more abrupt. They are connected with SPP wave scattering at the arms splitting point.

By changing the splitter geometry it is possible to create a splitter with different ratios between the signals in the output arms. The starting point with $d_{sp}=0$ in these simulations was the optimal symmetric splitter with a harmonic function shape of the arms [case (i)] and a length of 7.5 μm. Changing the symmetry of the splitter by shifting the input arm vertically from the symmetry axis by a distance of d_{sp} can provide splitting ratios up to ~1.6 [Fig. 6(a)]. In this case, coupling to the output arm placed closer to the position of the input waveguide will be more efficient. This provides a bigger signal in comparison with the other arm. The bigger the shift, the higher the ratio between the output arms signals. When the maximum shift $d_{sp}=D/2$ is reached, a further increase in the splitting ratio can be obtained by keeping the larger signal arm (so that they make a straight waveguide) and decreasing the length of the splitter region L_{sp} [Fig.

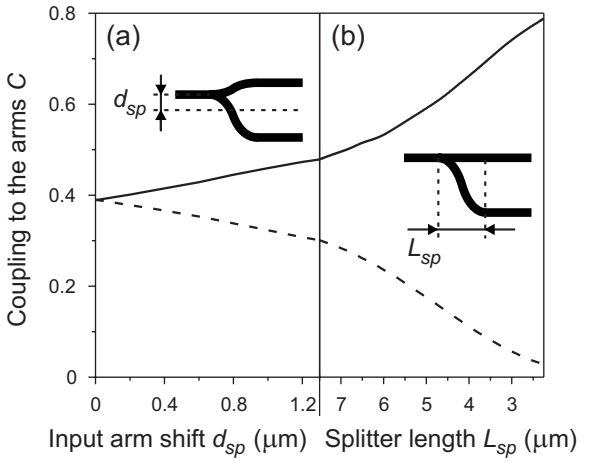

FIG. 6. Asymmetric splitter: dependence of the coupling efficiency into the splitter arms C on (a) input arm shift d_{sp} from the symmetric configuration (splitter length $L_{sp}=7.5$ μm) and (b) splitter length L_{sp}. The solid and dashed curves correspond to left and right arms, respectively.

6(b)]. The smaller the length, the more abrupt the branching of, and thus, the less efficient the coupling to it. Splitting ratios up to 30 can be easily implemented in these geometries. The total energy in both arms remains practically unchanged.

We also considered other designs of the splitter, particularly based on the tunnel-coupling mechanism between two parallel waveguides discussed above [see Fig. 2(b)]. For both designs we performed optimization of the geometry, trying different distances between the coupled waveguides and varying the coupling sections lengths. Such designs provide a similar level of splitting efficiency as observed in the case of fork-shaped splitter. However these designs require quite high fabrication accuracy. As we found earlier the coupling length dramatically depends on the distance between the waveguides, which, therefore, should be fabricated with a high precision on the order of tens of nanometers. Contrary, we found that the fabrication precision requirement for the fork-shaped splitter is much more feasible. For example, if the smallest feature of the waveguide at the arms splitting point will be roughened up to 300 nm, it will result in less than a 5% decrease in the coupling efficiency C.

C. Bragg reflectors

We studied different approaches for the implementation of a Bragg reflector in the DLSPP waveguide for each approach optimizing the geometrical parameters, such as the reflector period and aspect ratio. In the first instance, we considered the modulation of the waveguide dielectric stripe height up to the maximum value of $h_r/h=1$ [see Fig. 7(a)]. The width of the square wave a was chosen to be a half of the Bragg period calculated for unperturbed mode $P_{\mathrm{Bragg}}=\lambda_{\mathrm{SPP}}/2=\lambda/2\ \mathrm{Re}(n_{\mathrm{eff}})$, while the width of the gap b was varied to get the necessary 2π phase shift for the waves reflected from neighboring periods. This is necessary because the mode in the gap is not the same as the mode in the waveguide, having different field distributions and a different wave vector (effective refractive index). In this design, if a short reflector is required (e.g., we studied five-period reflector), large modulation amplitudes are needed because the mode is localized at the metal interface [see Fig. 2(b)]. However, in this case the gaps in the waveguide become efficient SPP scatterers due to the mode profile difference between a waveguide full-height mode and the mode in the gaps. This limits the reflectivity of such a reflector at the level of $R\sim 0.5$. We also implemented Bragg reflector on the basis of square-wave or sinusoidal modulation of the refractive index of the stripe up to a modulation amplitude of 20% [Figs. 7(b) and 7(c)]. We optimized the designs by varying the width of the denser dielectric in the first case (keeping the width of the conventional section $P_{\mathrm{Bragg}}/2$) and the period of the modulation (around P_{Bragg}) in the second case. As before, this optimization is required because the mode wave vector in the regions of optically denser dielectric is larger then the mode wave vector in the conventional waveguide. The length of the reflector was set to be 20 periods. We found that reflectors of these designs can provide reasonably high reflectivity of $R\sim 0.7-0.8$ at refractive index modulation of 20%. However, such high refractive index modulation is experimentally challenging, while at low modulation magnitudes the reflectors need to be rather long.

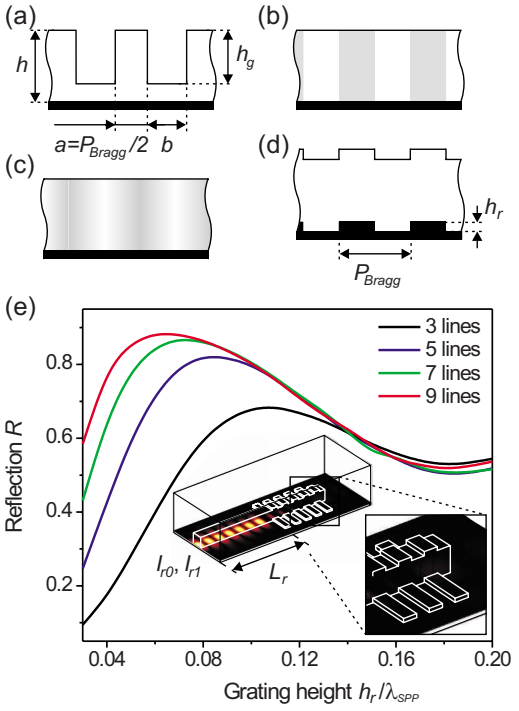

FIG. 7. (Color online) Bragg reflector based on (a) periodic modulation of the waveguide height, (b) square-wave and (c) sinusoidal modulations of the dielectric refractive index, and (d) rectangular metallic grating on the surface of metal. (e) Dependence of reflectivity R of the rectangular metallic grating on the grating height h_r for different number of periods. The inset shows the simulation setup.

From all the studied approaches for Bragg reflector, the best performance and the compact size were realized using a metallic stripe Bragg grating deposed at the metal-dielectric waveguide interface [Fig. 7(d) and inset of Fig. 7(e)]. Practically it can be created by first deposing the grating and then fabricating the waveguide. In this geometry in the first approximation, the mode propagates with the wave vector $k=2\pi n_{\mathrm{eff}}/\lambda$, so we set the period of the grating to be P_{Bragg}. We tried several gratings with a different number of periods for each case, optimizing the grating height h_r. The reflectivity was calculated using the power flow integrals in the dielectric cores of the waveguide $R=(I_{r0}-I_{r1})/[I_{r0}\exp(-2L_r/L_{\mathrm{prop}})]$. Here I_{r0} is the integral of the power flow of the incident wave and I_{r1} is the measured power flow taking into account the reflected SPP wave. We also checked the obtained values of reflectivity by analyzing the interference pattern produced by the incident and reflected SPP waves. The reflectivity values from these two approaches was found to be in a good agreement. We found [see Fig. 7(e)] that as much as 88% of the SPP mode, energy can be reflected by the Bragg metallic grating having just nine lines. The length of the reflector is just $9P_{\mathrm{Bragg}}\approx 11\ \mu\mathrm{m}$.

IV. GAIN DIELECTRIC AND LOSSLESS DLSPPW

Although SPPs provide very good localization of the optical signal, the signal propagation length is finite. For all the

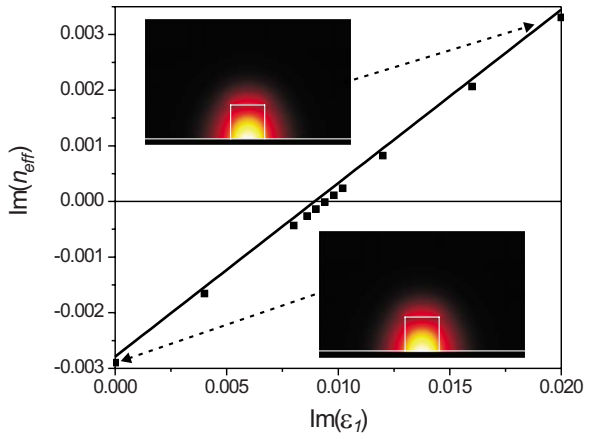

FIG. 8. (Color online) Dependence of the imaginary part of the effective refractive index of the SPP mode on the imaginary part of the dielectric constant of polymer, responsible for amplification. The line corresponds to the results of 2D eigenmode simulations and the symbols to the results of full 3D simulations. The insets show the abs(E_y) field maps for no-gain ($\epsilon_1=2.36$) and amplifying ($\epsilon_1=2.36+0.01866i$) cases.

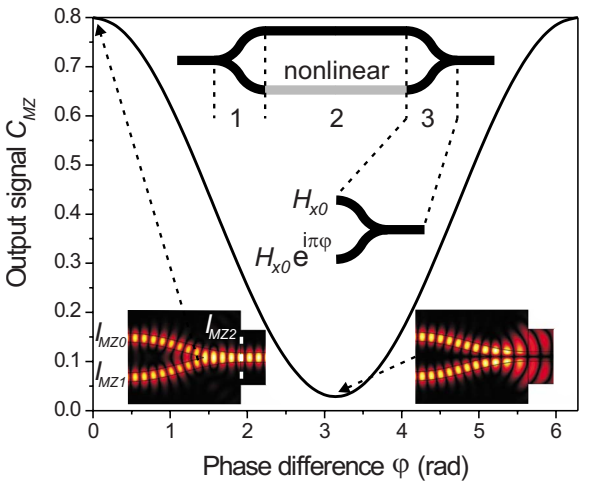

FIG. 9. (Color online) Mach-Zehnder interferometer: dependence of the output signal in the coupling part (3) on the phase difference in the arms. The insets show the abs(E_y) field maps for the cases of constructive and destructive interference.

SPP guiding approaches, there is a trade-off between the localization and the propagation length. It is related to the fact that in the case of strong localization, bigger part of the SPP mode field is located in metal, and thus the mode experience higher Ohmic losses. In the case of DLSPP waveguide considered here, the propagation length is $L_{\text{prop}}\sim 44$ μm. One of the possible solutions to increase the propagation length is to use a dielectric having an optical gain instead of the conventional dielectric media.[11,27] This idea is supported by the fact that a planar laser with internal mechanism solely based on SPPs amplification has already been proposed.[28,29]

The approach of using a gain medium can be naturally realized in the case of DLSPPW by doping the dielectric with quantum dots, or alternatively with lasing atoms or molecules. To find out the magnitude of amplification required in order to achieve lossless mode propagation, we studied the dependence of the mode propagation on the gain in the dielectric. The gain was phenomenologically introduced by adding an amplifying imaginary part to the dielectric constant. Particularly we studied the imaginary part of the effective refractive index of the mode $\text{Im}(n_{\text{eff}})$, which is in charge of the mode damping or amplification $L_{\text{prop}}=\lambda/[2\pi\,\text{Im}(n_{\text{eff}})]$, as shown in Fig. 8. The solid curve represents the 2D eigenmode simulations, while the points correspond to the 3D simulation results. The slight difference in values is due to the fact that in 2D simulations, we could afford much denser mesh, and thus the simulation accuracy although the overall agreement between 2D and 3D is very good. The lossless propagation of the mode corresponds to the point where $\text{Im}(n_{\text{eff}})=0$ ($L_{\text{prop}}=\infty$). It takes place at the gain corresponding to $\text{Im}(\epsilon_1)\approx 0.009$. To prove the validity of the result we estimate the requirement for lossless propagation on the semi-infinite metal-dielectric interface, defined by a simple relation, based on SPP dispersion expression: $\text{Im}(\omega/c[\epsilon_1\epsilon_2/(\epsilon_1+\epsilon_2)]^{1/2})=0$. This gives the gain value of $\text{Im}(\epsilon_1)\sim 0.004$. This value has the same order of magnitude as the one found for DLSPP waveguide. The difference is explained by two factors. In the case of DLSPPW, not all of the mode fields is located in the dielectric and amplified; at the same time, a larger part of the SPP field is located in the metal leading to higher Ohmic losses. The value of the gain required for lossless propagation of the mode corresponds to the gain coefficient $\gamma=2\pi/\lambda\times\text{Im}(\epsilon_1)/[\text{Re}(\epsilon_1)]^{1/2}\approx 249$ cm^{-1} or a gain of 108 dB/mm. This value of gain coefficient can be achieved using a gain medium based on quantum dots.[30] We found that the mode profiles are virtually the same in the cases of lossy and lossless mode propagation or even in the case of mode amplification (see insets of Fig. 8).

As a next step, we estimated the performance of the main passive waveguide components under condition of lossless propagation of the guided mode: $\text{Im}(\epsilon_1)\sim 0.00944$. These results are presented in Figs. 3–5 with curves labeled (b). In all the considered cases of bends and splitters their efficiency values reaches as much as ~95% with only about 5% being dissipated as radiation losses.

V. ACTIVE DLSPPW ELEMENTS

A. Mach-Zehnder interferometer

As the first example of active devices based on DLSPP waveguides, the performance of a Mach-Zehnder interferometer was estimated. One arm of the interferometer was made from the nonlinear material so that its refractive index can be changed upon illumination with control light. Thus, the phase difference in the arms can be produced and the output signal modulated, depending on constructive or destructive interference in the MZI output waveguide. Due to limitations connected with computational power we simulated it in steps. The performance of the splitting section 1 (see sketch in Fig. 9) has been studied above and we found that it can provide efficiency up to 78%. Section 1 is essentially the

propagation of the mode along the straight DLSPP waveguides. It leaves however the question about the SPP mode interaction with the interface between the materials of different refractive indices: between sections 1 and 2 as well as sections 2 and 3. Performing numerical simulations, we found that even for refractive index difference up to 10%, there is no noticeable reflection or scattering from the interfaces (less than ~2%). After that the only question remaining is interference of the SPP waves in the coupling area (section 3). Numerical simulations were performed for this section allowing the output signal to be monitored as a function of the phase difference, ϕ, gained in the arms, while the absolute power flow in the arms was maintained ($I_{MZ0}=I_{MZ1}$) (see Fig. 9). We found that when there is no phase difference and the interference of the signals is constructive, the normalized output power flow $C_{MZ}=I_{MZ2}/(I_{MZ0}+I_{MZ1})$ is as much as 0.8. On the other hand, when the difference is π and the interference is destructive, there is a negligibly small signal in the output arm $C_{MZ}=0.024$. This leads to modulation contrast of the interferometer $(C^0_{MZ}-C^\pi_{MZ})/(C^0_{MZ}+C^\pi_{MZ})=0.93$. Analyzing the field maps (see the insets of Fig. 9), we can see that when the interference is destructive for the SPP modes in the output waveguide, the interference is constructive for the fields scattered outside the waveguide. In these regions the optical path difference for the signals in the input arms has a constructive value. As a consequence, no considerable reflection (less then few percent) back in the MZI arms was observed as the phase difference in the arms ϕ is changed.

B. Amplifying and modulating element

Finally, we estimated the performance of an active element inserted in a waveguide, which can play a role of amplifying and modulating element. We implemented it as a 10 μm section of the material in which the gain can be induced by an external pumping. The gain level $\mathrm{Im}(\epsilon_2)=0.01866$ was chosen to be the twice the SPP propagation losses in the conventional waveguide. This value is not twice the value for lossless propagation because of the gain dependence in Fig. 8 is slightly nonlinear. As can be expected, under such conditions, the power in the amplifying section increases at the same rate with which it is absorbed in the conventional waveguide sections (Fig. 10). Moreover the amplification starts from the same value of power flow with which the mode reaches the sections interface. This means that there is negligible scattering of the guided mode at this interface. This was also confirmed by the calculations of integrals of power flow directed out of the waveguide. The absence of scattering is not surprising since the mode profiles are very similar in the conventional waveguide and in the amplifying section (see the mode profiles in Fig. 8). As a consequence, the SPP wave naturally transforms from one mode to the other. Similar behavior of the SPP modes in the case of metallic strip waveguide embedded in conventional and amplifying dielectric was observed in Ref. 11.

VI. SUMMARY AND CONCLUSIONS

In conclusion, using full 3D numerical simulations, we characterized a wide range of passive and active waveguide elements on the basis of dielectric-loaded SPP waveguides. The results show that a very high photonic integration density can be achieved with a distance between the waveguides just ~2 μm at the telecommunication wavelength range. We demonstrated efficient waveguide bends, splitters, and Bragg reflectors of various designs. For each design the performance of the element has been optimized, varying its geometrical parameters. The efficiency of the all the optimal elements was found to be as much as 75%–85%, with their functional size being in the range of just several micrometers for telecommunication wavelengths. We have found the criterion for the lossless propagation of the mode in the waveguide and determined the performance of the DLSPPW lossless elements. With lossless propagation the transmission efficiency of the elements rises up to 95%. Finally, we have estimated the performance of DLSPPW active elements: Mach-Zehnder interferometer as well as SPP amplifying and modulating elements. Such DLSPPW photonic elements are extremely beneficial in comparison with conventional planar waveguide technology, which can provide similar loss parameters only in millimeter length scale of bend elements and can find applications in photonic and optoelectronic integrated circuits and lab-on-a-chip sensing.

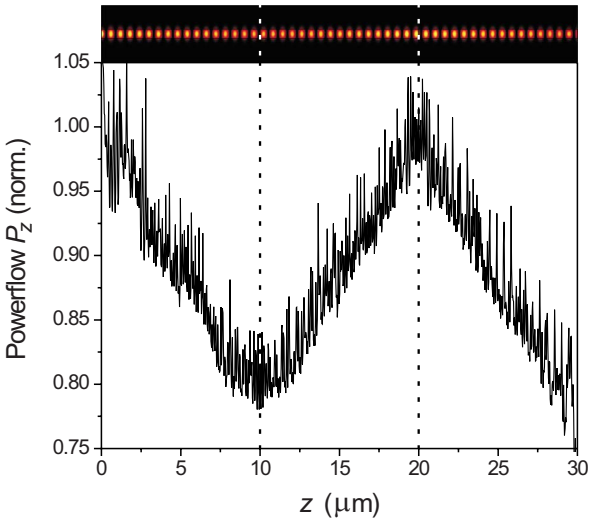

FIG. 10. (Color online) Dependence of the power flow P_z along the DLSPP waveguide with an optical gain section. The dielectric constant of the gain section $\epsilon_1=2.36+0.01866i$ provides the gain allowing to compensate losses in the waveguide section of the same length made of conventional dielectric with $\epsilon_1=2.36$.

ACKNOWLEDGMENTS

This work was supported in part by EPSRC (United Kingdom) and EC FP6 STREP PLASMOCOM. The authors acknowledge the fruitful discussions with G. A. Wurtz, S. I. Bozhevolnyi, and P. Bayvel.

*a.krasavin@qub.ac.uk

[1] H. Raether, *Surface Plasmons on Smooth and Rough Surfaces and Gratings* (Springer-Verlag, Berlin, 1988).
[2] A. Zayats, I. Smolyaninov, and A. Maradudin, Phys. Rep. **408**, 131 (2005).
[3] J. Krenn and J.-C. Weeber, Philos. Trans. R. Soc. London, Ser. A **362**, 739 (2004).
[4] J. Takahara, S. Yamagishi, H. Taki, A. Morioto, and T. Kabayashi, Opt. Lett. **22**, 475 (1997).
[5] T. Nikolajsen, K. Leosson, and S. Bozhevolnyi, Appl. Phys. Lett. **85**, 5833 (2004).
[6] S. Bozhevolnyi, V. Volkov, E. Devaux, J.-Y. Laluet, and T. Ebbesen, Nature (London) **440**, 508 (2006).
[7] L. Chen, B. Wang, and G. P. Wang, Appl. Phys. Lett. **89**, 243120 (2006).
[8] M. Yan and M. Qiu, J. Opt. Soc. Am. B **24**, 2333 (2007).
[9] S. A. Maier and H. A. Atwater, J. Appl. Phys. **98**, 011101 (2005).
[10] B. Wang and G. Wang, Appl. Phys. Lett. **90**, 013114 (2007).
[11] M. Nezhad, K. Tetz, and Y. Feinman, Opt. Express **12**, 4072 (2004).
[12] A. V. Krasavin and N. I. Zheludev, Appl. Phys. Lett. **84**, 1416 (2004).
[13] D. Pacifici, H. J. Lezec, and H. A. Atwater, Nat. Photonics **1**, 402 (2007).
[14] I. I. Smolyaninov, A. V. Zayats, A. Stanishevsky, and C. C. Davis, Phys. Rev. B **66**, 205414 (2002).
[15] W. Dickson, G. A. Wurtz, P. R. Evans, R. J. Pollard, and A. V. Zayats, Nano Lett. **8**, 281 (2008).
[16] A. Degiron, C. Dellagiacoma, J. G. McIlhargey, G. Shvets, O. J. F. Martin, and D. R. Smith, Opt. Lett. **32**, 2354 (2007).
[17] P. Berini, R. Charbonneau, S. Jetté-Charbonneau, N. Lahoud, and G. Mattiussi, J. Appl. Phys. **101**, 113114 (2007).
[18] C. Reinhardt, S. Passinger, B. Chichkov, C. Marquart, I. Radko, and S. Bozhevolnyi, Opt. Lett. **31**, 1307 (2006).
[19] B. Steinberger, A. Hohenau, H. Ditlbacher, A. L. Stepanov, A. Drezet, F. Aussenegg, A. Leitner, and J. Krenn, Appl. Phys. Lett. **88**, 094104 (2006).
[20] T. Holmgaard and S. I. Bozhevolnyi, Phys. Rev. B **75**, 245405 (2007).
[21] A. V. Krasavin and A. V. Zayats, Appl. Phys. Lett. **90**, 211101 (2007).
[22] T. Holmgaard, S. I. Bozhevolnyi, L. Marker, and A. Dereux, Appl. Phys. Lett. **92**, 011124 (2008).
[23] S. Massenot, J. Grandidier, A. Bouhelier, G. C. des Francs, J.-C. W. L. Markey, A. Dereux, J. Renger, M. U. Gonzàlez, and R. Quidant, Appl. Phys. Lett. **91**, 243102 (2007).
[24] A. Seidel, C. Ohrt, S. Passinger, C. Reinhardt, R. Kiyan, and B. Chichkov (unpublished).
[25] *Handbook of Optical Constants of Solids*, edited by E. D. Palik (Academic, New York, 1984).
[26] A. Kumar and S. Aditya, Microwave Opt. Technol. Lett. **19**, 289 (1998).
[27] J. Seidel, S. Grafstrom, and L. Eng, Phys. Rev. Lett. **94**, 177401 (2005).
[28] M. Bahriz, V. Moreau, J. Palomo, R. Colombelli, D. A. Austin, J. W. Cockburn, L. R. Wilson, A. B. Krysa, and J. S. Roberts, Appl. Phys. Lett. **88**, 181103 (2006).
[29] T. Okamoto, F. H'Dhili, and S. Kawata, Appl. Phys. Lett. **85**, 3968 (2004).
[30] P. Berini, SPP3, Abstract book p. 194 (2007).